Thermoelectric properties in semimetals with inelastic electron-hole scattering

Keigo Takahashi [1,*] Hiroyasu Matsuura [1] Hideaki Maebashi [1] and Masao Ogata [1,2]

[1]*Department of Physics, University of Tokyo, 7-3-1 Hongo, Bunkyo, Tokyo 113-0033, Japan*
[2]*Trans-Scale Quantum Science Institute, University of Tokyo, 7-3-1 Hongo, Bunkyo, Tokyo 113-0033, Japan*

We present systematic theoretical results on thermoelectric effects in semimetals based on the variational method of the linearized Boltzmann equation. Inelastic electron-hole scattering is known to play an important role in the unusual transport of semimetals, including the broad T^2 temperature dependence of the electrical resistivity and the strong violation of the Wiedemann-Franz law. By treating the inelastic electron-hole scattering more precisely beyond the relaxation-time approximation, we show that the Seebeck coefficient when compensated depends on the screening length of the Coulomb interaction as well as the Lorenz ratio (the ratio of thermal to electric conductivity due to electrons divided by temperature). It is found that deviations from the compensation condition significantly increase the Seebeck coefficient, along with crucial suppressions of the Lorenz ratio. The result indicates that uncompensated semimetals with the electron-hole scattering have high thermoelectric efficiency when the phonon contribution to thermal conductivity is suppressed.

I. INTRODUCTION

Thermoelectric effect or the Seebeck effect, which induces the electromotive force by a temperature gradient, has attracted much attention from the perspective of energy harvesting. The efficiency of the power generation due to the thermoelectric effect is expressed by a dimensionless figure of merit, $ZT \equiv S^2 \sigma T / (\kappa_{el} + \kappa_{ph})$, where S, σ, κ_{el} (κ_{ph}), and T are the Seebeck coefficient, electrical conductivity, thermal conductivity of electrons (phonons), and temperature, respectively. Materials with large ZT have potential applications in power supplies and thermoelectric cooling.

Conducting materials can be broadly classified into three categories according to their transport properties: metals, semiconductors, and semimetals [1]. Metals have the highest electrical conductivity, but they also have proportionally high thermal conductivity and usually satisfy the Wiedemann-Franz (WF) law, which states that the Lorenz ratio ($L = \kappa_{el}/\sigma T$) becomes the universal constant $L_0 = \pi^2 k_B^2 / 3e^2$ with $e < 0$ being the charge of an electron. The WF law prevents metals from having large ZT. In general, materials that exhibit high thermoelectric performance belong to semiconductors with a large Seebeck coefficient. Thermoelectricity of semimetals, the third category of conducting materials with intermediate conductivity between that of metals and semiconductors, has also been studied for many years [2–5], and has recently attracted renewed interest [6–11].

The electronic transport due to the electron-hole scattering in semimetals shows several intriguing phenomena, even if the energy dispersion of the model is simple as in Fig. 1. First, the electron-hole scattering gives a T^2 temperature dependence of the electrical resistivity even without the umklapp process [4,12–17]. This is because momentum conservation does not necessarily lead to velocity conservation in the case of semimetals. Second, recent experimental and theoretical studies on WP$_2$ have revealed a downward violation of the WF law [18–22], in which the Lorenz ratio becomes small depending on the screening length of the Coulomb interaction. This is due to the fact that the thermal current is more strongly relaxed than the electrical current due to electron-hole scattering, an effect that goes beyond the relaxation-time approximation (RTA) in transport theory. Since the dimensionless figure of merit ZT can be rewritten as

$$ZT = \frac{S^2}{L + \kappa_{ph}/\sigma T}, \tag{1}$$

an unusually small Lorenz ratio in semimetals can lead to a large figure of merit.

In this paper, we systematically study the thermoelectric properties of semimetals using a simple but standard model to clarify the dependencies of the electrical, thermal, and thermoelectric transport coefficients on (i) the carrier numbers (compensated, electron-doped, and hole-doped), (ii) the effective masses of electrons and holes, and (iii) the screening length of the Coulomb interaction. In the previous studies, the Lorenz ratio in a compensated semimetal was studied by exact solutions of the Boltzmann equation [20,22]. However, this method is not valid for the thermoelectric coefficients. The thermoelectric coefficients due to the electron-hole scattering were studied only for the compensated case by the RTA [22]. Therefore, the general behavior of thermoelectric coefficients for the uncompensated semimetal with the electron-hole scattering is unclear. In addition, the RTA is not exact for inelastic scattering [1] and the importance of inelastic scattering in a semimetal has been discussed [10]. Therefore, it should be testified whether the RTA is valid or not by the analysis beyond RTA. Analysis by the trial functions is useful to consider transports in the presence of the inelastic scattering and employed in various systems, such as graphene and bilayer graphene [23–25]. Here, we apply the variational method [2]

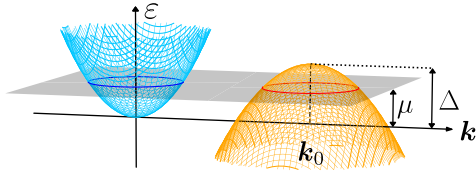*takahashi@hosi.phys.s.u-tokyo.ac.jp

115158-1

FIG. 1. Two-band model consisting of electron (blue) and hole (orange) bands.

to the linearized Boltzmann equation, which is more reliable than RTA. We will show that there is a contribution to the thermoelectric effect that is not captured by the RTA in the previous study. In the present paper, we focus on the effect of the electron-hole scattering, and the effect of phonons is out of the scope of this paper [26]. In the following, we study the temperature range $k_B T/\Delta \lesssim 0.06$ where Δ is an energy offset (see Fig. 1) since the electron-hole scattering becomes dominant in low-temperature region compared to the electron-phonon scattering.

This paper is organized as follows. In Sec. II, we introduce the model and the Boltzmann equation. In particular, in Sec. II A, we provide a detailed description of our model, illustrated in Fig. 1. In Sec. II B, we introduce a systematic method based on the Boltzmann equation to calculate the transport coefficients for this model. The results and discussions are given in Sec. III. First, we present the temperature dependence of transport coefficients. Then, we discuss the carrier-number dependence of thermoelectric properties when the electron-hole scattering dominates. In the compensated case, the Seebeck coefficient is zero if the effective masses of the electrons and holes are the same. If the effective masses are different, the Seebeck coefficient becomes finite, but small. However, we will show that it is sensitive to the screening length of the Coulomb interaction as is the case for the Lorenz ratio. In the uncompensated cases, we find that slight deviations from the compensation bring a large Seebeck coefficient when the electron-hole scattering dominates. We also estimate $\widetilde{ZT} \equiv S^2 \sigma T/\kappa_{el} = S^2/L$, which gives an upper bound of the figure of merit, in our framework, and find that the electron-hole scattering gives large $\widetilde{ZT}$ in the uncompensated case due to the collaboration of the reduction of the Lorenz ratio and the increase of the Seebeck coefficient. Finally, the conclusions are given in Sec. IV.

II. MODEL AND BOLTZMANN EQUATION

A. Model

We study a two-band model depicted in Fig. 1 consisting of electron and hole bands with three-dimensional quadratic dispersions [20,22]

$$\varepsilon_{1,\boldsymbol{k}} = \frac{\hbar^2 \boldsymbol{k}^2}{2m_1}, \quad \varepsilon_{2,\boldsymbol{k}} = \Delta - \frac{\hbar^2 (\boldsymbol{k} - \boldsymbol{k}_0)^2}{2m_2}, \quad (2)$$

where m_1 (m_2) is the effective mass of electrons (holes), and Δ is the energy offset. Therefore, both carriers have spherical Fermi surfaces.

The number of electrons (holes) is given by $n_1 = V^{-1}\sum_{\boldsymbol{k}} 2f_0(\varepsilon_{1,\boldsymbol{k}})$ ($n_2 = V^{-1}\sum_{\boldsymbol{k}} 2[1 - f_0(\varepsilon_{2,\boldsymbol{k}})]$) where a factor 2 and V indicate the spin degeneracy, and the volume

of the system, and $f_0(\varepsilon) = (e^{\beta(\varepsilon-\mu)} + 1)^{-1}$ is the Fermi-Dirac distribution function with $\beta = (k_B T)^{-1}$ and μ is the chemical potential which keeps the net charge $e\Delta n = e(n_1 - n_2)$ at the value of $T = 0$. By introducing a parameter χ defined by $k_{F,2} = \chi k_{F,1}$, we obtain $n_2 = \chi^3 n_1$ at $T = 0$ and the Fermi energy (ε_F) is given by $\varepsilon_F = m_2 \Delta/(\chi^2 m_1 + m_2)$. As a typical scale of wave number, we define $k_F = \sqrt{2m_1 m_2 \Delta/\hbar^2(m_1 + m_2)}$, which is the Fermi wave number in the case of $\chi = 1$, which corresponds to the compensated case, $n_1 = n_2$.

B. Boltzmann equation and variational method

The Boltzmann equation of the system is given by [2,20,22]

$$\left[-eE_x v_{\boldsymbol{k};x}^{(l)} - (\varepsilon_{l,\boldsymbol{k}} - \mu)v_{\boldsymbol{k};x}^{(l)}\left(-\frac{\nabla_x T}{T}\right) \right]\left(-\frac{\partial f_0(\varepsilon_{l,\boldsymbol{k}})}{\partial \varepsilon_{l,\boldsymbol{k}}}\right)$$
$$= \left(\frac{\partial f^{(l)}(\boldsymbol{k})}{\partial t}\right)_{\text{imp}} + \left(\frac{\partial f^{(l)}(\boldsymbol{k})}{\partial t}\right)_{\text{e-h}} + \left(\frac{\partial f^{(l)}(\boldsymbol{k})}{\partial t}\right)_{\text{e-e}}, \quad (3)$$

where $v_{\boldsymbol{k};x}^{(l)} = \hbar^{-1}\nabla_{k_x}\varepsilon_{l,\boldsymbol{k}}$ ($l = 1, 2$) is the velocity of the band l ($l = 1, 2$). E_x and $(-\nabla_x T/T)$ are the electric field and the temperature gradient along the x axis, respectively. The three terms on the right-hand side of Eq. (3) represent the impurity, interband (electron-hole), and intraband (electron-electron and hole-hole) scattering, respectively. We assume that the impurity scattering is due to the short-range impurity potential and the inter- and intraband scattering are due to the screened Coulomb interaction where we neglect the exchange process [20,22]. For example, the electron-hole scattering for the band $l = 1$ is given by [20,22]

$$\left(\frac{\partial f^{(1)}(\boldsymbol{k})}{\partial t}\right)_{\text{e-h}} = -2 \sum_{\boldsymbol{k}_2,\boldsymbol{k}_3,\boldsymbol{k}_4} S_{\text{e-h}}(\boldsymbol{k},\boldsymbol{k}_2;\boldsymbol{k}_3,\boldsymbol{k}_4)f^{(1)}(\boldsymbol{k})f^{(2)}(\boldsymbol{k}_2)$$
$$\times [1 - f^{(1)}(\boldsymbol{k}_3)][1 - f^{(2)}(\boldsymbol{k}_4)]$$
$$+ 2 \sum_{\boldsymbol{k}_1,\boldsymbol{k}_2,\boldsymbol{k}_4} S_{\text{e-h}}(\boldsymbol{k}_1,\boldsymbol{k}_2;\boldsymbol{k},\boldsymbol{k}_4)f^{(1)}(\boldsymbol{k}_1)f^{(2)}(\boldsymbol{k}_2)$$
$$\times [1 - f^{(1)}(\boldsymbol{k})][1 - f^{(2)}(\boldsymbol{k}_4)], \quad (4)$$

where the factor 2 is the spin degeneracy and $S_{\text{e-h}}(\boldsymbol{k}_1,\boldsymbol{k}_2;\boldsymbol{k}_3,\boldsymbol{k}_4)$ is given by

$$S_{\text{e-h}}(\boldsymbol{k}_1,\boldsymbol{k}_2;\boldsymbol{k}_3,\boldsymbol{k}_4) = \frac{2\pi}{\hbar}\frac{1}{V^2}\left(\frac{1}{4\pi\varepsilon_0}\right)^2\left(\frac{4\pi e^2}{|\boldsymbol{k}_1 - \boldsymbol{k}_3|^2 + \alpha^2}\right)^2$$
$$\times \frac{(2\pi)^3}{V}\delta(\boldsymbol{k}_1 + \boldsymbol{k}_2 - \boldsymbol{k}_3 - \boldsymbol{k}_4)$$
$$\times \delta(\varepsilon_{1,\boldsymbol{k}_1} + \varepsilon_{2,\boldsymbol{k}_2} - \varepsilon_{1,\boldsymbol{k}_3} - \varepsilon_{2,\boldsymbol{k}_4}). \quad (5)$$

Here, ε_0 is the dielectric constant and α represents the inverse of the Thomas-Fermi screening length, where $\alpha^2 = e^2(m_1 k_{F,1} + m_2 k_{F,2})/\pi^2 \hbar^2 \varepsilon_0$ [20,22]. The other scattering terms have similar forms, which are given in Appendix A.

In the variational method [2], the distribution function is expanded as $f^{(l)}(\boldsymbol{k}) = f_0(\varepsilon_{l,\boldsymbol{k}}) + \beta f_0(\varepsilon_{l,\boldsymbol{k}})[1 - f_0(\varepsilon_{l,\boldsymbol{k}})]\Phi^{(l)}(\boldsymbol{k})$ where $\Phi^{(l)}$ is assumed to be small. Keeping terms up to the first order of $\Phi^{(l)}$, Eq. (3) can be rewritten

as [2]

$$X^{(l)} = P^{(l)}[\Phi] = P_{\text{imp}}^{(l)}[\Phi] + P_{\text{e-h}}^{(l)}[\Phi] + P_{\text{e-e}}^{(l)}[\Phi], \quad (6)$$

where $-X^{(l)}$ denotes the left-hand side of Eq. (3). Note that $P_{\text{imp}}^{(l)}[\Phi]$ and $P_{\text{e-e}}^{(l)}[\Phi]$ are linear functionals of $\Phi^{(l)}$, while $P_{\text{e-h}}^{(l)}[\Phi]$ is a linear functional of $(\Phi^{(1)}, \Phi^{(2)})$. Explicit forms of these scattering terms are presented in Appendix A. Then, we assume that the trial function for the band l is given by $\Phi^{(l)}(\boldsymbol{k}) = \sum_{i=1}^{2} \eta_i^{(l)} \varphi_i^{(l)}(\boldsymbol{k})$, where $\varphi_i^{(l)}(\boldsymbol{k}) = v_{\boldsymbol{k};x}^{(l)}(\varepsilon_{l,\boldsymbol{k}} - \mu)^{i-1}$ and the coefficients $\eta_i^{(l)}$ are determined so as to maximize a variational functional. Using the variational method [2,27], we obtain the expression for $\eta_i^{(l)}$ as

$$\eta_i^{(l)} = \sum_{j,k} (P^{-1})_{ij}^{(lk)} \left[J_j^{(k)} E_x + U_j^{(k)} \left(-\frac{\nabla_x T}{T} \right) \right], \quad (7)$$

where $P_{ij}^{(lk)}$ is a matrix representation of $P^{(l)}[\Phi]$ for the chosen basis $\{\varphi_i^{(l)}(\boldsymbol{k})\}$ and

$$\begin{pmatrix} J_i^{(l)} \\ U_i^{(l)} \end{pmatrix} = \frac{1}{V} \sum_{\boldsymbol{k}} \varphi_i^{(l)}(\boldsymbol{k}) v_{\boldsymbol{k};x}^{(l)} \begin{pmatrix} e \\ \varepsilon_{l,\boldsymbol{k}} - \mu \end{pmatrix} \left(-\frac{\partial f_0(\varepsilon_{l,\boldsymbol{k}})}{\partial \varepsilon_{l,\boldsymbol{k}}} \right). \quad (8)$$

The explicit form of matrix $P_{ij}^{(lk)}$ is given in Appendix B. Since $P_{\text{e-h}}^{(l)}[\Phi]$ contains the distribution function of the other band, we have the superscript (lk) in $P_{ij}^{(lk)}$. In the evaluation of $P_{ij}^{(lk)}$, we analytically perform angular integrals, and numerically evaluate the remaining energy integrals. The details are given in the Supplemental Material (SM) [27]. Transport coefficients (L_{11}, $L_{12} = L_{21}$, and L_{22}), which relate the electric (heat) current J_x ($J_{q;x}$) to the external fields, defined as

$$\begin{pmatrix} J_x \\ J_{q;x} \end{pmatrix} = \begin{pmatrix} L_{11} & L_{12} \\ L_{21} & L_{22} \end{pmatrix} \begin{pmatrix} E_x \\ -\nabla_x T/T \end{pmatrix}, \quad (9)$$

are given by

$$\begin{pmatrix} L_{11} & L_{12} \\ L_{21} & L_{22} \end{pmatrix} = 2 \sum_{i,l,j,k} \begin{pmatrix} J_i^{(l)} \\ U_i^{(l)} \end{pmatrix} (P^{-1})_{ij}^{(lk)} \left(J_j^{(k)}, U_j^{(k)} \right). \quad (10)$$

In the degenerate regime ($k_B T \ll \varepsilon_F$), these transport coefficients are approximated as

$$L_{11} \simeq 2 \left({}^t\boldsymbol{J}_1 P_{11}^{-1} \boldsymbol{J}_1 \right), \quad (11)$$

$$L_{12} \simeq 2 \left[{}^t\boldsymbol{J}_1 P_{11}^{-1} \boldsymbol{U}_1 + \left({}^t\boldsymbol{J}_2 - {}^t\boldsymbol{J}_1 P_{11}^{-1} P_{12} \right) P_{22}^{-1} \boldsymbol{U}_2 \right], \quad (12)$$

$$L_{22} \simeq 2 \left({}^t\boldsymbol{U}_1 P_{11}^{-1} \boldsymbol{U}_1 + {}^t\boldsymbol{U}_2 P_{22}^{-1} \boldsymbol{U}_2 \right), \quad (13)$$

by considering the power of $k_B T/\varepsilon_F$ where $\boldsymbol{J}_i = {}^t(J_i^{(1)}, J_i^{(2)})$ and $\boldsymbol{U}_i = {}^t(U_i^{(1)}, U_i^{(2)})$. It should be noted that although ${}^t\boldsymbol{U}_1 P_{11}^{-1} \boldsymbol{U}_1$ in L_{22} is not the leading order, we consider this term because it corresponds to the ambipolar contribution [2,21,22].

III. RESULTS AND DISCUSSIONS

A. Temperature dependence

Figure 2 shows the temperature dependencies of resistivity $\rho = \sigma^{-1} = L_{11}^{-1}$, thermal conductivity $\kappa_{\text{el}} = (L_{22} - L_{21}L_{12}/L_{11})/T$, and the Seebeck coefficient $S = L_{12}/T L_{11}$ for
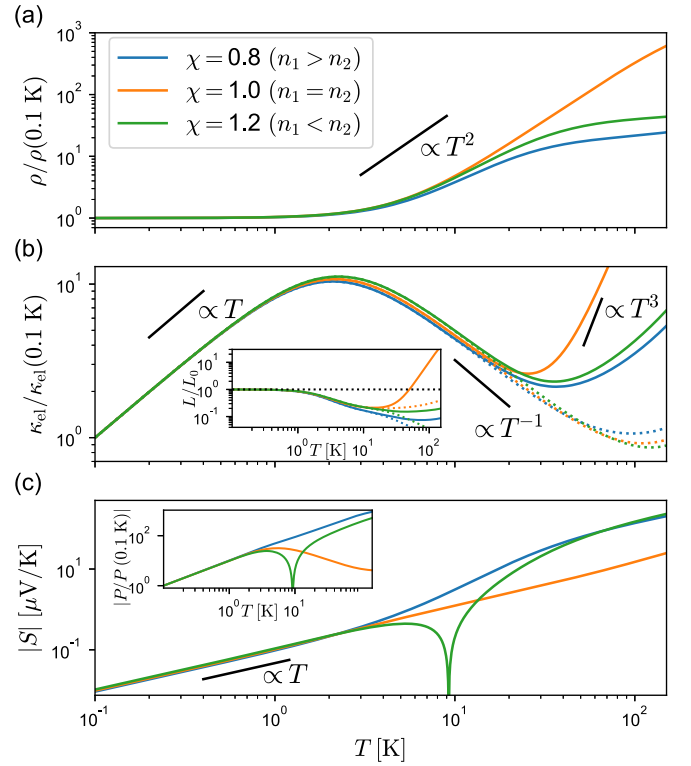

FIG. 2. Temperature dependencies of (a) electrical resistivity, (b) thermal conductivity, and (c) the absolute value of Seebeck coefficient for three values of χ with $m_2 = 3m_1 = 3m_e$. We normalize the electrical resistivity and thermal conductivity by the value at $T = 0.1$ K. The dotted lines in (b) represent $\tilde{\kappa}_{\text{el}}$ defined in the text. In (c), the Seebeck coefficient for $\chi = 1.2$ changes its sign at $T = 10$ K. The inset of (b) shows the temperature dependence of the normalized Lorenz ratio $L/L_0 = \kappa_{\text{el}}\rho/T L_0$ (solid lines) and $\tilde{\kappa}_{\text{el}}\rho/T L_0$ (dotted lines) with $L_0 = \pi^2 k_B^2/3e^2$. The inset of (c) indicates temperature dependence of the Peltier conductivity $P \equiv S\sigma$.

three values of χ. Lorenz ratio and Peltier conductivity $P \equiv S\sigma$ are also shown in the inset of (b) and (c), respectively. Here, we set $m_2 = 3m_1 = 3m_e$ with m_e being the electron mass and ε_0 so that $\alpha = k_F$ at $\chi = 1$. In the following, we use $\Delta = 0.2$ eV as a typical value. The strength of the impurity scattering is chosen so that the electron-hole scattering dominates above 4 K (see Appendix A for the choices of parameters).

1. Electrical resistivity

The electrical resistivity ρ [Fig. 2(a)] is independent of T in the region of $T \lesssim 4$ K, because the impurity scattering dominates. As temperature increases, ρ shows T^2 dependence due to the electron-hole scattering (4 K $\lesssim T \lesssim 30$ K). On the other hand, in high-temperature regime ($T \gtrsim 30$ K), ρ in the compensated case ($\chi = 1.0$) shows T^2 dependence, while ρ saturates in the uncompensated cases. This is because the contribution to the electric current from the total momentum, which is relaxed only through momentum dissipative scatterings, is proportional to $n_1 - n_2$, and this contribution does not vanish in the uncompensated case [13] (see also SM [27]). When the system is uncompensated and the relative

momentum is strongly relaxed by the electron-hole scattering, the relaxation of the total momentum by the impurity scattering governs the electric conduction [13,14,28]. Then, the saturated resistivity ρ_{sat} obeys $\rho_{sat}/\rho(T = 0) \sim [(n_1 + n_2)/(n_1 - n_2)]^2$ [13,27].

2. Thermal conductivity

The thermal conductivity κ_{el} [Fig. 2(b)] is proportional to T at low temperatures. As shown in the inset, WF law holds in this temperature region. In the intermediate temperature region, κ_{el} decreases slightly slower than to T^{-1}. This temperature dependence is approximately consistent with WF law ($\kappa_{el} \propto T\sigma$), but the normalized Lorenz ratio is less than 1 and temperature dependent.

For the compensated case ($\chi = 1$), this result is consistent with previous studies [20–22]. In particular, T^3 dependence is due to the ambipolar effect [21,22]. Actually, $\tilde{\kappa}_{el} \equiv 2(^tU_2 P_{22}^{-1} U_2)/T$ [dotted lines in Fig. 2(b)], which does not include the ambipolar contribution, does not show the increase but instead has the T^{-1} dependence in a wider range of temperatures. For $T > 60$ K, $\tilde{\kappa}_{el}$ upwardly deviates from T^{-1} due to the subleading temperature dependence [27].

In contrast, in the uncompensated case, κ_{el} does not follow T^3 dependence and is smaller than κ_{el} for $\chi = 1$. As a result, L/L_0 (inset) is small even in the high-temperature region. This means that the ambipolar contribution is not large when uncompensated. The ambipolar contribution is associated with the transport of the compensated electrons and holes moving in the same direction under the temperature gradient giving no electric current as discussed for semiconductors [2]. This ambipolar contribution is also present in semimetals [21,22] and is weak in the uncompensated case. We can show [27] that, in $\kappa_{el} = (L_{22} - L_{21}L_{12}/L_{11})/T$, the enhancement of L_{12} in the uncompensated case cancels the ambipolar contribution in L_{22} leading to the suppression of the Lorenz ratio.

3. Seebeck coefficient

The Seebeck coefficient S is negative and almost independent of χ in the low-temperature region. This is because the transport property is mainly determined by the electrons that have a smaller effective mass than the holes. In this low-temperature region, the impurity scattering is dominant and thus the Mott formula is valid. At higher temperatures, S for $\chi = 1.2$ changes its sign to positive at $T \sim 10$ K. This can be understood as follows. In the high-temperature region, the relative momentum between electrons and holes is strongly relaxed by the electron-hole scattering, and thus the electric current is mainly carried by the total momentum proportional to $e(n_1 - n_2)$ [13]. As a result, the sign of S is determined by the holes for the case of $\chi = 1.2$ ($n_2 > n_1$). In the temperature region above 40 K, S becomes again almost linear in T. Apparently, the coefficient of the linear T term for $\chi \neq 1$ is about ten times larger than that at low temperatures.

First, let us study the Seebeck coefficient for the compensated case ($\chi = 1$) more closely. We plot in Fig. 3 the temperature dependence of $|S/T|$ for three screening lengths. We can see that the coefficient of the linear-T term gradually increases as a function of T and reaches some value, which depends on α. The black dashed line in Fig. 3(a) shows
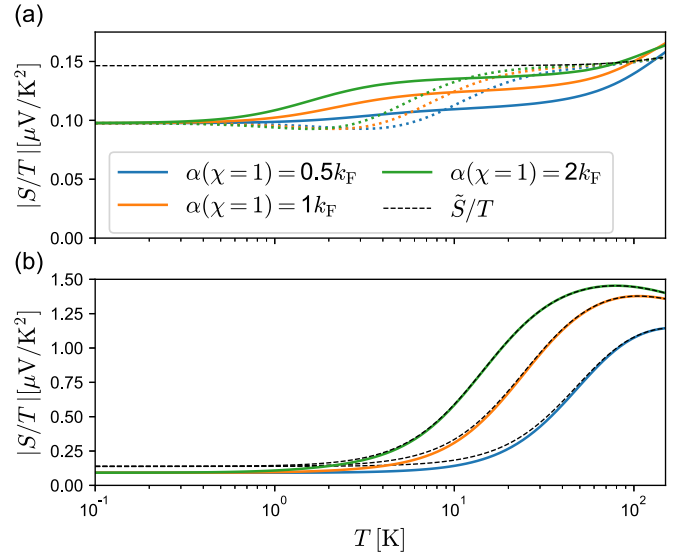

FIG. 3. Temperature dependencies of $|S/T|$ for three screening lengths, or equivalently three dielectric constants for (a) $\chi = 1$ and (b) $\chi = 0.8$. The dielectric constants are chosen so that $\alpha = 0.5k_F$, $1.0k_F$, and $2.0k_F$ at $\chi = 1$. Colored dotted lines in (a) show results when considering the impurity and intraband scattering.

$\tilde{S}/T \equiv {}^tJ_1 P_{11}^{-1} U_1/T^2({}^tJ_1 P_{11}^{-1} J_1)$, which is equivalent to the RTA as shown in the SM [27]. Apparently, $\tilde{S}/T$ does not depend on α, which is consistent with the previous study [22] showing that the Seebeck coefficient in the RTA does not depend on the relaxation time by the electron-hole scattering (see also the SM [27]). This indicates that the RTA does not explain the α dependence of S in Fig. 3 for the compensated case. To see the effect of the electron-hole scattering, we show the results (colored dotted lines in Fig. 3) in which the electron-hole scattering is neglected and only the impurity and intraband scattering are considered. In this case, $|S/T|$ in the high-temperature region does not depend on α, which means that the interband scattering plays an important role in α dependence of S. Since the first term of the right-hand side of Eq. (12) corresponds to the RTA [27], the α dependence comes from the other terms in Eq. (12), i.e., from the terms including P_{12} and P_{22}. In particular, P_{12} is nonzero for the electron-hole scattering unlike the intraband scattering.

For the uncompensated cases ($\chi \neq 1$), the situation is different. Figure 3(b) shows the temperature dependence of $|S/T|$ for three screening lengths in the case of $\chi = 0.8$. In this case, the enhancement of $|S/T|$ at high temperatures is larger than that for $\chi = 1$. In the uncompensated cases, ${}^tJ_1 P_{11}^{-1} U_1$ in Eq. (12) gives the major contribution when the electron-hole scattering dominates [27]. As a result, S can be approximated as $\tilde{S} = {}^tJ_1 P_{11}^{-1} U_1/T({}^tJ_1 P_{11}^{-1} J_1)$, which is equivalent to the RTA. In fact, $\tilde{S}/T$, which are shown in the black dashed lines in Fig. 3(b), reproduce S/T at high temperatures.

B. Carrier-number dependence

To understand the effect of doping and the difference in effective masses, we plot in Fig. 4 the χ dependence of the Seebeck coefficient, the Lorenz ratio (inset), and
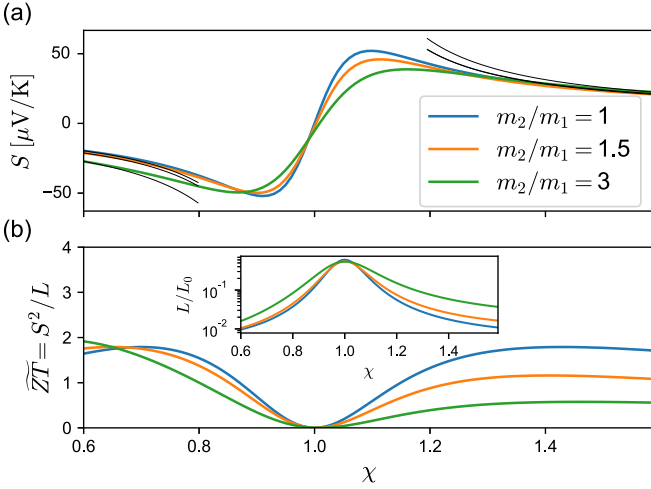
FIG. 4. χ dependencies of (a) Seebeck coefficient and (b) $\widetilde{ZT} = S^2\sigma T/\kappa_{\rm el} = S^2/L$ at 40 K. ε_0 is the same as in Fig. 2. The inset of (b) shows the Lorenz ratio. Black lines in (a) are proportional to $(m_1 + \chi m_2)(\chi^2 m_1 + m_2)/(\chi^3 - 1)$.

$\widetilde{ZT} = S^2\sigma T/\kappa_{\rm el} = S^2/L$ for three values of m_2/m_1 at $T =$ 40 K. We can see that the absolute value of S increases and the Lorenz ratio drastically decreases in the uncompensated case. As a result, $\widetilde{ZT}$ [Fig. 4(b)] drastically increases in the uncompensated case. For the case of $m_2/m_1 = 1$, $\widetilde{ZT}$ is almost symmetric with respect to χ, while $\widetilde{ZT}$ is larger for the case with $\chi < 1$, i.e., $n_1 > n_2$, than for the case with $\chi > 1$ when $m_2/m_1 > 1$. As we can see from Fig. 2(c), S at $T = 40$ K is almost the same for $\chi = 0.8$ and $\chi = 1.2$. Thus, the difference in $\widetilde{ZT}$ comes from the difference in the Lorenz ratio.

In the limit of vanishing the impurity scattering, the Seebeck coefficient behaves as $S \simeq \tilde{S} \sim (m_1 + \chi m_2)(\chi^2 m_1 + m_2)/(\chi^3 - 1) \propto (n_2 - n_1)^{-1}$ [27]. We see this dependence in the black lines of Fig. 4(a) for χ far away from 1. This means that a slight deviation from compensation can lead to a large Seebeck coefficient. As discussed in Ref. [14] in connection to the Hall coefficient, we can interpret the behavior of S as follows: the electrons and holes are locked by the electron-hole scattering and they can be treated as a single carrier with charge $e(n_1 - n_2)$. Note the present result is similar to that of the carrier-number dependence of the Seebeck coefficient in graphene and bilayer graphene [23,24]. Controlling carrier numbers to make a small deviation from compensation

is a strategy for the large Seebeck coefficient as observed in $Ti_{1+x}S_2$ [4,6]. Our results suggest that this strategy in clean semimetals with dominating electron-hole scattering is also beneficial for reducing the Lorenz ratio and then achieving high ZT.

IV. CONCLUSIONS

In the present paper, we studied the effects of electron-hole scattering with a finite screening length within the Boltzmann transport theory. However, when we consider the Kubo-Luttinger linear response theory in the case of the finite-range Coulomb interaction, there is an additional contribution in the heat current operator that does not satisfy the Sommerfeld-Bethe relation [29,30]. Since this type of heat current operator is not taken into account in the Boltzmann equation, the microscopic study based on the Kubo-Luttinger formalism might reveal a new aspect of transport in semimetals.

In conclusion, we have studied transport coefficients of semimetals considering the impurity, electron-hole, and intraband scattering based on the variational analysis of the Boltzmann equation. We have shown that the thermoelectric coefficient of semimetals with the electron-hole scattering contains contributions beyond the RTA. The part neglected in the RTA brings the screening lengths dependence of the Seebeck coefficient. We have also shown that when the electron-hole scattering dominates in the uncompensated cases the Seebeck coefficient is largely enhanced. $\widetilde{ZT}$, in which the phononic thermal conductivity is neglected, can be large in the uncompensated condition due to the increase of the Seebeck coefficient and the reduction of the Lorenz ratio. Although our analysis does not take into account $\kappa_{\rm ph}$, this semimetal system can be a very good candidate for thermoelectric devices.

APPENDIX A: SCATTERING TERMS

The scattering terms are presented. The impurity scattering is given by

$$\left(\frac{\partial f^{(l)}(\boldsymbol{k})}{\partial t}\right)_{\rm imp} = -\sum_{\boldsymbol{k}'} S_{\rm imp}^{(l)}(\boldsymbol{k}, \boldsymbol{k}')f^{(l)}(\boldsymbol{k})[1 - f^{(l)}(\boldsymbol{k}')] + \sum_{\boldsymbol{k}'} S_{\rm imp}^{(l)}(\boldsymbol{k}', \boldsymbol{k})f^{(l)}(\boldsymbol{k}')[1 - f^{(l)}(\boldsymbol{k})], \tag{A1}$$

where l represents the band $l = 1, 2$, and

$$S_{\rm imp}^{(l)}(\boldsymbol{k}', \boldsymbol{k}) = S_0 \delta(\varepsilon_{l,\boldsymbol{k}} - \varepsilon_{l,\boldsymbol{k}'}). \tag{A2}$$

S_0 determines the strength of the impurity scattering. We set $VS_0\tilde{k}_{\rm F}^3/4\pi^2 = 1.35 \times 10^{-11}$ J/s, where $\tilde{k}_{\rm F}$ is a Fermi wave number for $m_2 = 3m_1 = 3m_{\rm e}$, $\Delta = 0.2$ eV, and $\chi = 1$.

The electron-hole scattering for the band $l = 2$ is given by

$$
\left(\frac{\partial f^{(2)}(\boldsymbol{k})}{\partial t}\right)_{\text{e-h}} = -2 \sum_{\boldsymbol{k}_1, \boldsymbol{k}_3, \boldsymbol{k}_4} S_{\text{e-h}}(\boldsymbol{k}_1, \boldsymbol{k}; \boldsymbol{k}_3, \boldsymbol{k}_4) f^{(1)}(\boldsymbol{k}_1) f^{(2)}(\boldsymbol{k})[1 - f^{(1)}(\boldsymbol{k}_3)][1 - f^{(2)}(\boldsymbol{k}_4)]
$$

$$
+ 2 \sum_{\boldsymbol{k}_1, \boldsymbol{k}_2, \boldsymbol{k}_3} S_{\text{e-h}}(\boldsymbol{k}_1, \boldsymbol{k}_2; \boldsymbol{k}_3, \boldsymbol{k}) f^{(1)}(\boldsymbol{k}_1) f^{(2)}(\boldsymbol{k}_2)[1 - f^{(1)}(\boldsymbol{k}_3)][1 - f^{(2)}(\boldsymbol{k})]. \tag{A3}
$$

The intraband scattering for the band l is given by

$$
\left(\frac{\partial f^{(l)}(\boldsymbol{k})}{\partial t}\right)_{\text{e-e}} = -2 \sum_{\boldsymbol{k}_2, \boldsymbol{k}_3, \boldsymbol{k}_4} S_{\text{e-e}}^{(l)}(\boldsymbol{k}, \boldsymbol{k}_2; \boldsymbol{k}_3, \boldsymbol{k}_4) f^{(l)}(\boldsymbol{k}) f^{(l)}(\boldsymbol{k}_2)[1 - f^{(l)}(\boldsymbol{k}_3)][1 - f^{(l)}(\boldsymbol{k}_4)]
$$

$$
+ 2 \sum_{\boldsymbol{k}_1, \boldsymbol{k}_2, \boldsymbol{k}_4} S_{\text{e-e}}^{(l)}(\boldsymbol{k}_1, \boldsymbol{k}_2; \boldsymbol{k}, \boldsymbol{k}_4) f^{(l)}(\boldsymbol{k}_1) f^{(l)}(\boldsymbol{k}_2)[1 - f^{(l)}(\boldsymbol{k})][1 - f^{(l)}(\boldsymbol{k}_4)] \tag{A4}
$$

and

$$
S_{\text{e-e}}^{(l)}(\boldsymbol{k}_1, \boldsymbol{k}_2; \boldsymbol{k}_3, \boldsymbol{k}_4) = \frac{2\pi}{\hbar} \frac{1}{V^2} \left(\frac{1}{4\pi\varepsilon_0}\right)^2 \left(\frac{4\pi e^2}{|\boldsymbol{k}_1 - \boldsymbol{k}_3|^2 + \alpha^2}\right)^2 \frac{(2\pi)^3}{V} \delta(\boldsymbol{k}_1 + \boldsymbol{k}_2 - \boldsymbol{k}_3 - \boldsymbol{k}_4) \delta(\varepsilon_{l,\boldsymbol{k}_1} + \varepsilon_{l,\boldsymbol{k}_2} - \varepsilon_{l,\boldsymbol{k}_3} - \varepsilon_{l,\boldsymbol{k}_4}), \tag{A5}
$$

where we use the same screened Coulomb potential as in $S_{\text{e-h}}(\boldsymbol{k}_1, \boldsymbol{k}_2; \boldsymbol{k}_3, \boldsymbol{k}_4)$.

The linearized forms of scattering terms are given by

$$
P_{\text{imp}}^{(l)}[\Phi] = \frac{1}{k_B T} \sum_{\boldsymbol{k}'} S_{\text{imp}}^{(l)}(\boldsymbol{k}', \boldsymbol{k}) f_0(\varepsilon_{l,\boldsymbol{k}})[1 - f_0(\varepsilon_{l,\boldsymbol{k}'})][\Phi^{(l)}(\boldsymbol{k}) - \Phi^{(l)}(\boldsymbol{k}')], \tag{A6}
$$

$$
P_{\text{e-h}}^{(1)}[\Phi] = \frac{2}{k_B T} \sum_{\boldsymbol{k}_2, \boldsymbol{k}_3, \boldsymbol{k}_4} S_{\text{e-h}}(\boldsymbol{k}_1, \boldsymbol{k}_2; \boldsymbol{k}_3, \boldsymbol{k}_4) f_0(\varepsilon_{1,\boldsymbol{k}_1}) f_0(\varepsilon_{2,\boldsymbol{k}_2})[1 - f_0(\varepsilon_{1,\boldsymbol{k}_3})][1 - f_0(\varepsilon_{2,\boldsymbol{k}_4})]
$$

$$
\times [\Phi^{(1)}(\boldsymbol{k}_1) + \Phi^{(2)}(\boldsymbol{k}_2) - \Phi^{(1)}(\boldsymbol{k}_3) - \Phi^{(2)}(\boldsymbol{k}_4)], \tag{A7}
$$

$$
P_{\text{e-h}}^{(2)}[\Phi] = \frac{2}{k_B T} \sum_{\boldsymbol{k}_1, \boldsymbol{k}_3, \boldsymbol{k}_4} S_{\text{e-h}}(\boldsymbol{k}_1, \boldsymbol{k}_2; \boldsymbol{k}_3, \boldsymbol{k}_4) f_0(\varepsilon_{1,\boldsymbol{k}_1}) f_0(\varepsilon_{2,\boldsymbol{k}_2})[1 - f_0(\varepsilon_{1,\boldsymbol{k}_3})][1 - f_0(\varepsilon_{2,\boldsymbol{k}_4})]
$$

$$
\times [\Phi^{(1)}(\boldsymbol{k}_1) + \Phi^{(2)}(\boldsymbol{k}_2) - \Phi^{(1)}(\boldsymbol{k}_3) - \Phi^{(2)}(\boldsymbol{k}_4)], \tag{A8}
$$

$$
P_{\text{e-e}}^{(l)}[\Phi] = \frac{2}{k_B T} \sum_{\boldsymbol{k}_2, \boldsymbol{k}_3, \boldsymbol{k}_4} S_{\text{e-e}}^{(l)}(\boldsymbol{k}_1, \boldsymbol{k}_2; \boldsymbol{k}_3, \boldsymbol{k}_4) f_0(\varepsilon_{l,\boldsymbol{k}_1}) f_0(\varepsilon_{l,\boldsymbol{k}_2})[1 - f_0(\varepsilon_{l,\boldsymbol{k}_3})][1 - f_0(\varepsilon_{l,\boldsymbol{k}_4})]
$$

$$
\times [\Phi^{(l)}(\boldsymbol{k}_1) + \Phi^{(l)}(\boldsymbol{k}_2) - \Phi^{(l)}(\boldsymbol{k}_3) - \Phi^{(l)}(\boldsymbol{k}_4)]. \tag{A9}
$$

APPENDIX B: MATRIX $P_{ij}^{(lk)}$

The matrix $P_{ij}^{(lk)}$ is understood as a matrix representation of the scatterings. This is given by $P_{ij}^{(lk)} = P_{\text{imp},ij}^{(lk)} + P_{\text{e-h},ij}^{(lk)} + P_{\text{e-e},ij}^{(lk)}$ where

$$
P_{\text{imp},ij}^{(lk)} = \frac{\delta_{lk}}{2k_B TV} \sum_{\boldsymbol{k}, \boldsymbol{k}'} S_{\text{imp}}^{(l)}(\boldsymbol{k}, \boldsymbol{k}') f_0(\varepsilon_{l,\boldsymbol{k}})[1 - f_0(\varepsilon_{l,\boldsymbol{k}'})][\varphi_i^{(l)}(\boldsymbol{k}) - \varphi_i^{(l)}(\boldsymbol{k}')][\varphi_j^{(l)}(\boldsymbol{k}) - \varphi_j^{(l)}(\boldsymbol{k}')], \tag{B1}
$$

$$
P_{\text{e-h},ij}^{(11)} = \frac{1}{k_B TV} \sum_{\boldsymbol{k}_1, \boldsymbol{k}_2, \boldsymbol{k}_3, \boldsymbol{k}_4} S_{\text{e-h}}(\boldsymbol{k}_1, \boldsymbol{k}_2; \boldsymbol{k}_3, \boldsymbol{k}_4) f_0(\varepsilon_{1,\boldsymbol{k}_1}) f_0(\varepsilon_{2,\boldsymbol{k}_2})[1 - f_0(\varepsilon_{1,\boldsymbol{k}_3})][1 - f_0(\varepsilon_{2,\boldsymbol{k}_4})]
$$

$$
\times [\varphi_i^{(1)}(\boldsymbol{k}_1) - \varphi_i^{(1)}(\boldsymbol{k}_3)][\varphi_j^{(1)}(\boldsymbol{k}_1) - \varphi_j^{(1)}(\boldsymbol{k}_3)], \tag{B2}
$$

$$
P_{\text{e-h},ij}^{(12)} = P_{\text{e-h},ji}^{(21)} = \frac{1}{k_B TV} \sum_{\boldsymbol{k}_1, \boldsymbol{k}_2, \boldsymbol{k}_3, \boldsymbol{k}_4} S_{\text{e-h}}(\boldsymbol{k}_1, \boldsymbol{k}_2; \boldsymbol{k}_3, \boldsymbol{k}_4) f_0(\varepsilon_{1,\boldsymbol{k}_1}) f_0(\varepsilon_{2,\boldsymbol{k}_2})[1 - f_0(\varepsilon_{1,\boldsymbol{k}_3})][1 - f_0(\varepsilon_{2,\boldsymbol{k}_4})]
$$

$$
\times [\varphi_i^{(1)}(\boldsymbol{k}_1) - \varphi_i^{(1)}(\boldsymbol{k}_3)][\varphi_j^{(2)}(\boldsymbol{k}_2) - \varphi_j^{(2)}(\boldsymbol{k}_4)], \tag{B3}
$$

$$
P_{\text{e-h},ij}^{(22)} = \frac{1}{k_B TV} \sum_{\boldsymbol{k}_1, \boldsymbol{k}_2, \boldsymbol{k}_3, \boldsymbol{k}_4} S_{\text{e-h}}(\boldsymbol{k}_1, \boldsymbol{k}_2; \boldsymbol{k}_3, \boldsymbol{k}_4) f_0(\varepsilon_{1,\boldsymbol{k}_1}) f_0(\varepsilon_{2,\boldsymbol{k}_2})[1 - f_0(\varepsilon_{1,\boldsymbol{k}_3})][1 - f_0(\varepsilon_{2,\boldsymbol{k}_4})]
$$

$$
\times [\varphi_i^{(2)}(\boldsymbol{k}_2) - \varphi_i^{(2)}(\boldsymbol{k}_4)][\varphi_j^{(2)}(\boldsymbol{k}_2) - \varphi_j^{(2)}(\boldsymbol{k}_4)], \tag{B4}
$$

$$P_{\text{e-e},ij}^{(lk)} = \frac{\delta_{lk}}{2k_B TV} \sum_{\boldsymbol{k}_1,\boldsymbol{k}_2,\boldsymbol{k}_3,\boldsymbol{k}_4} S_{\text{e-e}}^{(l)}(\boldsymbol{k}_1,\boldsymbol{k}_2;\boldsymbol{k}_3,\boldsymbol{k}_4) f_0(\varepsilon_{l,\boldsymbol{k}_1}) f_0(\varepsilon_{l,\boldsymbol{k}_2})[1 - f_0(\varepsilon_{l,\boldsymbol{k}_3})][1 - f_0(\varepsilon_{l,\boldsymbol{k}_4})]$$

$$\times \left[\varphi_i^{(l)}(\boldsymbol{k}_1) + \varphi_i^{(l)}(\boldsymbol{k}_2) - \varphi_i^{(l)}(\boldsymbol{k}_3) - \varphi_i^{(l)}(\boldsymbol{k}_4) \right] \left[\varphi_j^{(l)}(\boldsymbol{k}_1) + \varphi_j^{(l)}(\boldsymbol{k}_2) - \varphi_j^{(l)}(\boldsymbol{k}_3) - \varphi_j^{(l)}(\boldsymbol{k}_4) \right]. \tag{B5}$$

[1] N. W. Ashcroft and N. D. Mermin, *Solid State Physics* (Holt, Rinehart and Winston, New York, 1976).

[2] J. M. Ziman, *Electrons and Phonons* (Oxford University Press, Oxford, 2001).

[3] K. Sugihara, J. Phys. Soc. Jpn. **27**, 356 (1969).

[4] A. H. Thompson, Phys. Rev. Lett. **35**, 1786 (1975).

[5] K. Durczewski and M. Ausloos, Z. Phys. B **85**, 59 (1991).

[6] M. Beaumale, T. Barbier, Y. Bréard, G. Guelou, A. V. Powell, P. Vaqueiro, and E. Guilmeau, Acta Mater. **78**, 86 (2014).

[7] B. Skinner and L. Fu, Sci. Adv. **4**, eaat2621 (2018).

[8] M. Markov, S. E. Rezaei, S. N. Sadeghi, K. Esfarjani, and M. Zebarjadi, Phys. Rev. Mater. **3**, 095401 (2019).

[9] F. Han, N. Andrejevic, T. Nguyen, V. Kozii, Q. T. Nguyen, T. Hogan, Z. Ding, R. Pablo-Pedro, S. Parjan, B. Skinner, A. Alatas, E. Alp, S. Chi, J. Fernandez-Baca, S. Huang, L. Fu, and M. Li, Nat. Commun. **11**, 6167 (2020).

[10] H. Takahashi, K. Hasegawa, T. Akiba, H. Sakai, M. S. Bahramy, and S. Ishiwata, Phys. Rev. B **100**, 195130 (2019).

[11] A. Nakano, A. Yamakage, U. Maruoka, H. Taniguchi, Y. Yasui, and I. Terasaki, J. Phys. Energy **3**, 044004 (2021).

[12] W. G. Baber, Proc. R. Soc. London, Ser. A **158**, 383 (1937).

[13] C. A. Kukkonen and P. F. Maldague, Phys. Rev. Lett. **37**, 782 (1976).

[14] C. A. Kukkonen and P. F. Maldague, Phys. Rev. B **19**, 2394 (1979).

[15] P. F. Maldague and C. A. Kukkonen, Phys. Rev. B **19**, 6172 (1979).

[16] J. Oliva and N. W. Ashcroft, Phys. Rev. B **25**, 223 (1982).

[17] D. T. Morelli and C. Uher, Phys. Rev. B **30**, 1080 (1984).

[18] J. Gooth, F. Menges, N. Kumar, V. Süß, C. Shekhar, Y. Sun, U. Drechsler, R. Zierold, C. Felser, and B. Gotsmann, Nat. Commun. **9**, 4093 (2018).

[19] A. Jaoui, B. Fauqué, C. W. Rischau, A. Subedi, C. Fu, J. Gooth, N. Kumar, V. Süß, D. L. Maslov, C. Felser, and K. Behnia, npj Quantum Mater. **3**, 64 (2018).

[20] S. Li and D. L. Maslov, Phys. Rev. B **98**, 245134 (2018).

[21] M. Zarenia, A. Principi, and G. Vignale, Phys. Rev. B **102**, 214304 (2020).

[22] W.-R. Lee, K. Michaeli, and G. Schwiete, Phys. Rev. B **103**, 115140 (2021).

[23] M. Zarenia, A. Principi, and G. Vignale, 2D Mater. **6**, 035024 (2019).

[24] M. Zarenia, T. B. Smith, A. Principi, and G. Vignale, Phys. Rev. B **99**, 161407(R) (2019).

[25] D. X. Nguyen, G. Wagner, and S. H. Simon, Phys. Rev. B **101**, 035117 (2020).

[26] Phonons may give two contributions. One is the electron-phonon scattering. This can be incorporated by adding a scattering term. The other is the thermal conductivity of phonons κ_{ph}, which we neglect in the estimation of the figure of merit in this paper.

[27] See Supplemental Material at http://link.aps.org/supplemental/10.1103/PhysRevB.107.115158 for detailed calculations and discussions of the variational method and the relaxation-time approximation, which include the discussions of the saturated resistivity, the subleading temperatures dependence, the ambipolar contribution, and a correspondence between the variational method and the relaxation-time approximation.

[28] H. K. Pal, V. I. Yudson, and D. L. Maslov, Lith. J. Phys. **52**, 142 (2012).

[29] M. Ogata and H. Fukuyama, J. Phys. Soc. Jpn. **88**, 074703 (2019).

[30] S. Takarada, M. Ogata, and H. Matsuura, Phys. Rev. B **104**, 165122 (2021).